Available online at www.sciencedirect.com
ScienceDirect
Journal of Photochemistry and Photobiology A: Chemistry 197 (2008) 402–414
Journal of Photochemistry and Photobiology A:Chemistry
www.elsevier.com/locate/jphotochem

Controlling J aggregation in fluorescein by bile salt hydrogels

Susmita Das, Asoke P. Chattopadhyay, Swati De *

Department of Chemistry, University of Kalyani, Kalyani 741 235, Nadia, West Bengal, India

Received 12 October 2007; received in revised form 10 January 2008; accepted 7 February 2008
Available online 14 February 2008

Abstract

Aggregation of the well-known xanthene dye, fluorescein has been studied in the restricted environment of a bile salt hydrogel and in the bile salt micelles. It has been observed that the hydrogel can be used to some extent "control" the type of aggregation in fluorescein, since J-aggregate formation is favored at the expense of H-aggregates in the gel. In contrast to the hydrogel, the effect of normal bile salt micelles is less dramatic, i.e., bile salt micelles do not lead to significant change in the type of dye aggregation.

Keywords: Fluorescein; Hydrogel; Aggregation; J-aggregates; H-aggregates

1. Introduction

Bile salts are steroidal detergents, which together with lipids/fats/cholesterol form mixed micelles in the intestine thus enabling digestion and absorption of fat [1,2]. Apart from micelles, bile salts also form hydrogels close to natural pH, i.e., pH ∼6 [3–9]. Gel formation in aqueous media, by polymers is very well documented [10], whereas gelation in bile salts has been studied by a few groups only [7–9]. The main difference between polymeric gels and bile salt gels is that for polymers, gelation occurs principally by chemical cross-linking of polymeric chains [10]. But gelation for molecular gels such as those formed by bile salts involves molecular self-assembly through non-covalent physical forces [8]. Apart from bile salts, other compounds like amino acid derivatives [11], polypeptides [12] carbohydrate derivatives [13], bola amphiphiles and gemini surfactants [14] can also act as gelators for aqueous fluids.

Unlike conventional surfactants, bile salts possess a rigid steroid backbone having polar hydroxyl groups on the concave α-face and methyl groups on the convex β-face. This imparts a unique facial amphiphilicity enabling aggregation of bile salts in aqueous solution via non-covalent physical forces—mainly hydrophobic association of the apolar β-faces of the steroid backbone, whereas further aggregation occurs through hydrogen bonding interactions [1–4]. Estroff and Hamilton [11a] have indicated that hydrophobic forces play a key role during gelation. Morphological examination [9,15] of the gel by cryo-TEM shows a network structure composed of sub-micron fibers forming an entangled mesh. Viscosity measurements [9b] indicate the viscosity around the fibers to be ∼120 cP which lends support to the entangled network picture. By monitoring the fluorescence of the polarity probe ANS in hydrogel environment, Maitra et al. [9,15] have shown that the gelation process creates highly hydrophobic pockets in an aqueous environment as fluorescence of ANS increases considerably in the gel medium indicating increased hydrophobicity around ANS.

Hydrogels are important because they are potential materials for biomedical applications, such as drug-delivery systems [16], tissue engineering, etc. Recently, Tiller has reviewed the advantages of using molecular hydrogels over polymeric gels [17]. Since these gels have potential use for applications involving gel encapsulated drugs and biomolecules, it is important to understand the internal environment in these gels. For this, fluorescence studies using a dye label may prove to be useful. Other workers have performed fluorescence studies on hydrogels [9,15] formed by bile salts. However, there the focus was on dynamic behavior of bound dyes in the constrained environment within the gel [3]. We have in the past studied aggregation behavior of xanthene dyes in various media [18]. Also some workers have observed enhanced J aggregation of a cyanine dye in restricted media, e.g., hectorite clay [19] and in PVA [20]. So, it was our keen interest to study the effect of gelation

* Corresponding author. Tel.: +919831244131; fax: +91 33 25828282.
E-mail address: swati_de1@rediffmail.com (S. De).

1010-6030/$ – see front matter © 2008 Elsevier B.V. All rights reserved.
doi:10.1016/j.jphotochem.2008.02.003

(i.e. restricted environment) on the aggregation of a well-known xanthene dye fluorescein (FL).

Dye aggregates are generally categorized into H-aggregates and J-aggregates. Dye aggregation is well treated by the exciton theory of Kasha and El-Bayoumi [21]. According to this theory, the *N*-fold degenerate singlet excited states of *N*-dye molecules in the aggregate are split into *N*-sublevels. Transitions from the ground state to any of the split-excited states may occur, subject to geometry restrictions in the aggregate. For H-aggregates, i.e., those in which monomers are arranged in parallel card-pack manner, only the transition to the topmost split level is allowed and hence the aggregate absorption/excitation spectrum is blue shifted with respect to the monomer. For J-aggregates, i.e., those in which the monomers are arranged in a head-to-tail manner, only transition to the lowest split level is allowed and hence the spectrum is red shifted with respect to the monomer. For aggregates having intermediate geometry, both these transitions are partially allowed and band splitting is observed. The J-aggregates of cyanine dyes are promising candidates for opto-electronic device applications [22]. They have important applications in photographic films, in solar energy conversion and in modeling energy transfer in photosynthetic antenna pigments [23,24].

It is also known from the contribution of a few workers that the gelation of bile salts results in H^+ uptake from the bulk media thus increasing the local pH of the media [7b]. We were also interested in probing this H^+ uptake during the gelation process using a pH sensitive probe. FL suits very well to this requirement. We focused on the hydrogel formed by the dihydroxy bile salt, sodium deoxycholate (NaDC), as NaDC hydrogels are commonly used for controlled drug delivery [25a].

2. Experimental

Fluorescein and NaDC were purchased from Fluka and were used as such. Double distilled water was used to prepare the solutions and Tris buffer was used to maintain the pH 6 and 8.3. Hydrogels of NaDC were prepared by adding measured amount of solid NaDC to the buffered solution of FL at pH 6 and then left to gelate for 45 min. Micelles of NaDC were prepared by adding measured amount of solid NaDC to the buffered FL solution at pH 8.3.

The steady state fluorescence studies were done with a Perkin Elmer spectrofluorimeter, LS-50B. The solutions were excited at 490 nm for emission studies. For recording the excitation spectra, λ_{em} was fixed at 555 nm. The UV–visible absorption spectra were measured with a Shimadzu UV 1601 PC spectrophotometer (Kyoto, Japan) in a 1 cm quartz cuvette. Fluorescence lifetimes were determined from time-resolved intensity decays by the method of time correlated single photon counting (TCSPC) using a diode (IBH, UK) nanoLED-07 as the light source at 403 nm. The full width at half maxima (FWHM) of this excitation source is 70 ps. The decay curves were analyzed using IBH-6 decay analysis software. The decays were given both single exponential and bi-exponential fits and depending on the χ^2 values and the residuals it was decided to be either single or bi-exponential. The steady-state fluorescence anisotropy (r) was calculated according to the relation $r = (I_{II} - I_L)/(I_{II} + 2I_L)$ where I_{II} and I_L are the vertically and horizontally polarized emission intensities, respectively.

Dynamic light scattering studies were performed with a Nano-ZS (Malvern) instrument, which is equipped with a 4-mW He–Ne laser ($\lambda = 632$ nm). The solutions for this study were prepared by filtering the Tris buffer (0.05 M) through a Whatman 42 filter paper and then weighed amount of sodium deoxycholate was added to prepare the gels and micelles of required concentration. The pH of the solution was maintained at 6 for the formation of gels and 8.3 for the formation of bile salt micelles. A glass cuvette of pathlength 1 cm, transparent on four sides was used. Scattered light was detected at 90° relative to the incident beam. A photo multiplier detected time-dependent fluctuations in the scattered light intensity. The operating procedure was programmed using Dispersion Technology Systems (DTS) software. There was an average of 30 runs, each run being averaged for 15 s. A mathematical process called "correlation" was carried out. The autocorrelation function $C(t)$ is actually the ensemble average of the product of the signal with a delayed version of itself as a function of delay time. At short delay, the correlation is high and with time (as the particles diffuse) correlation decreases to zero via an exponential decay. Analysis of the autocorrelation function in terms of the particle size distribution is done by fitting the data with calculations based on assumed distributions. For scattering from particles executing translational diffusion, $C(t)$ is given by $C(t) = \exp(-\tau/D)$, τ being the relaxation time and D the translational diffusion coefficient of the particles. D in turn is used to determine the mean hydrodynamic radius (R_h) through the Stokes' Einstein equation. Ultimately, the result is presented as a distribution of R_h. The peak and half-width of the distribution represent the mean Stokes' radius and its variation, respectively. The resolution of the experimental setup is 0.6 nm. Qualitative assessment about the structures was made using a Carl Zeiss Axioskop2 Plus fluorescence microscope. Analysis was done at 40× resolution. The lowest detection limit was 0.5 μm. The light source used in the microscope is a 35-W halogen lamp. The absorption spectra were resolved using the specwin 32 program, based on the principal component analysis (PCA) method [25b].

We have tried to arrive at the geometry-optimized structures for the dye aggregates. For this, the structure of the neutral dye molecule was drawn using CS Chem3D Ultra (Version 7.0.0, 2001). This was considered for geometry optimization (in the gas phase) at the AM1 level using the GAMESS-US program suite (Version September 7, 2006 R4) [26a]. Calculations based on density functional theory (DFT) were carried out on the AM1-optimized structure with valence-only SBKJC bases (and corresponding pseudo-potentials) [26b] and B3LYP functional [26c] using the same program. The lowest few excitation energies were obtained on the same structure using the time dependent density functional theory (TDDFT) method using the same basis set and exchange correlation functional [26b]. Calculations on the dianion were performed using the same procedure as the neutral dye monomer. For dimers, several sample structures were first generated by the CS Chem3D Ultra (Version 7.0.0, 2001). These were subjected to molecular dynamics

(MD) simulations using the same software. Suitable samples representing H-type and J-type dimers were further subjected to geometry optimization at the AM1 level and subsequently TDDFT calculations were performed on these.

3. Results

The motivation for this work was to study the effect of constrained environment (within the gel network), on the aggregation behavior of FL. For this purpose, the studies were performed at different dye concentrations. FL concentrations used were in the range 1×10^{-6} to 1×10^{-3} M. To compare the effect on FL aggregation by the NaDC hydrogel and normal NaDC micelles, all experimental studies were performed under two conditions: (1) in aqueous NaDC at pH 6—gelating condition and (2) in aqueous NaDC solutions at pH 8.3—non-gelating condition.

3.1. Studies in NaDC hydrogel

In aqueous buffer (pH 6), the absorption spectra of 1×10^{-6} to 1×10^{-5} M FL shows a prominent peak at 487 nm with a shoulder at 460 nm. On adding increasing concentration of NaDC (10–40 mM) gelation of the medium occurs with significant change of the absorption spectra of FL. The height of the 487 nm peak increases while the 460 nm shoulder becomes less prominent. We have performed PCA of the absorption spectra of 7×10^{-6} M FL in gel. In our case, PCA was done using wavelength scale. However, we have also performed PCA using energy scale and have obtained similar results by both methods. PCA reveals that the absorption spectra at these low-dye concentrations can be resolved into two components with peaks at 487 and 460 nm (Fig. 1a). Following earlier assignment [18a], the component at 487 nm is assigned to monomer dianion absorption. The 460 nm component needs to be assigned. PCA also reveals that in the gel, with increasing bile salt concentration, the amplitude of the longer wavelength component increases while the amplitude of 460 nm absorption decreases. This happens for low-dye concentrations, i.e., in the micromolar range.

For moderately high-dye concentrations, i.e., in the range above 1×10^{-5} M to less than 1×10^{-4} M, the absorption spectra show the characteristic peak at 487 nm with a shoulder at 460 nm. In presence of increasing gel concentration, the shoulder becomes less prominent while the 487 nm peak increases (Fig. 1b). PCA analysis of the absorption spectra yields two components at 500 and 455 nm, the components showing similar trends with increasing gel concentration, as observed earlier. Thus, we can see that for low to moderately high-dye concentrations, the effect of gelation on the absorption spectra of FL is same, only the contributing spectral components lie at shifted wavelengths.

For dye concentrations higher than 1×10^{-4} up to 1×10^{-3} M, the absorption spectra are inherently broad and no distinct peaks are visible. Addition of NaDC leads to increased absorbance in the shorter wavelength region, i.e., ~400–470 nm. PCA analyses show that at these high-dye concentrations, the absorption spectra can be resolved into two components at ~505 and 450 nm. Thus, the monomer peak is absent; instead we have a sharp red-shifted peak and a broader blue-shifted peak. Such a red-shifted sharp peak in absorbance is usually assigned to J-aggregates [19,21,27]. In our earlier work we have assigned such species in fluorescein, to Type B aggregates having J-type geometry [18a]. The blue-shifted broad absorption band had been assigned to Type A aggregates having H-type geometry. The Type A aggregates absorb at 450 nm for higher dye concentrations, indicating formation of higher aggregates (trimers, tetramers, etc.) compared to those existing at low-dye concen-

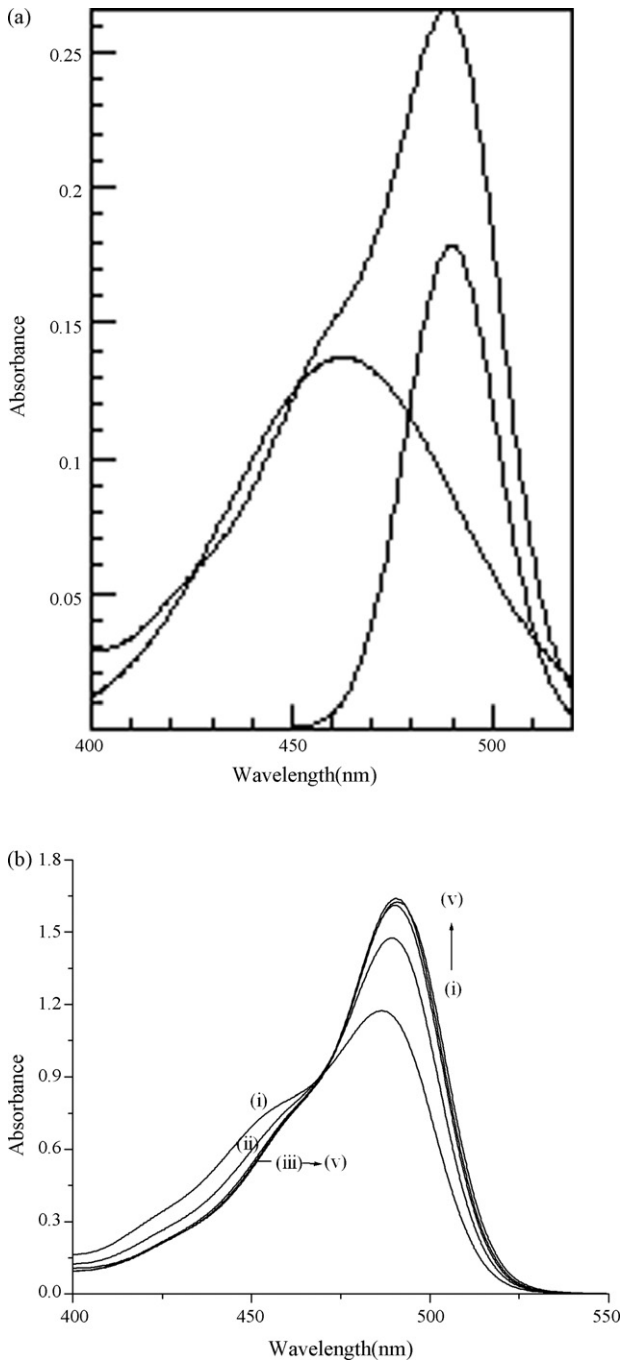

Fig. 1. (a) PCA resolved spectra of 7×10^{-6} M FL at pH 6. (b) Absorption spectra of 3×10^{-5} M FL with varying NaDC at pH 6: (i) 0 mM NaDC, (ii) 10 mM NaDC, (iii) 20 mM NaDC, (iv) 30 mM NaDC, and (v) 40 mM NaDC.

Table 1
Angles (θ) of FL aggregates in NaDC gel at pH 6

[FL] (M)	[NaDC] (mM)	f_1	f_2	f_1/f_2	$\theta = 2\tan^{-1}\sqrt{(f_1/f_2)}$
7×10^{-6}	0	0.240	0.460	0.522	71.7°
	10	0.280	0.350	0.800	83.7°
	20	0.288	0.341	0.845	85.2°
5×10^{-5}	0	0.238	0.484	0.492	70.1°
	10	0.305	0.427	0.714	80.4°
	20	0.316	0.409	0.773	82.7°
	30	0.311	0.434	0.716	80.5°
1×10^{-3}	0	0.183	0.682	0.265	54.8°
	10	0.157	0.618	0.258	53.9°
	20	0.133	0.548	0.243	52.5°
	30	0.125	0.506	0.247	52.9°

f_1 = oscillator strength of the longer wavelength component; f_2 = oscillator strength of the shorter wavelength component.

trations ($\lambda_{max}^{abs} = 460$ nm). PCA analysis also reveals that in neat dye solution, for higher dye concentrations ($>5 \times 10^{-5}$ M) both Type A and Type B aggregates contribute to the total absorbance.

The angle (θ) between the individual chromophores in the aggregates can be calculated as follows [18a,21]:

$$\theta = 2\ \tan^{-1}\sqrt{\left(\frac{f_1}{f_2}\right)} \quad (1)$$

where f_1 = oscillator strength of the longer wavelength component; f_2 = oscillator strength of the shorter wavelength component.

Since FL is not a linear molecule, in our case θ cannot be referred to as twist angle in the true sense. Rather it is the angle between the individual chromophores in the aggregate. The geometry-optimized structures of the FL molecule, both neutral form and the dianion are shown in Scheme 1. The highest occupied molecular orbital (HOMO) and lowest unoccupied molecular orbital (LUMO) of the dye molecule are both π orbitals of the anthracene moiety. The LUMO + 1 and LUMO + 2 are π orbitals of the benzoic acid unit, nearly orthogonal to the plane of the anthracene. While HOMO-1 is another π-type orbital of anthracene, HOMO-2 is mostly on the benzoic acid unit, as a π orbital of the latter.

The calculated values of θ and the corresponding oscillator strengths f_1 and f_2 are listed in Table 1. The procedure involved spectral deconvolution. Although it is known that spectral deconvolution often gives non-unique results, in our case the results were unique. Table 1 shows that $f_1 < f_2$ at all fluorescein concentrations. This implies that at aggregating concentrations, the H-type aggregates (absorbing at shorter wavelengths) predominate. However, for low to moderately high-dye concentrations, in presence of gel, f_1 increases and f_2 decreases progressively indicating that the gel medium preferentially enhances J-type or head-to-tail aggregation (corresponding to the longer wavelength component). For very high-dye concentrations, f_1/f_2 is low in concurrence with predominance of stacking or H-type aggregation at high-dye concentrations as reported in literature [18a,21]. We find that the θ for the neat dye solutions decreases as dye concentration increases. For a perfect H-aggregate θ should be 0° and for a perfect J-aggregate it should be 180° [19,21,27]. Lopez Arbeloa et al. obtained θ values of 74° for J-type aggregates of R3B in Hectorite clay and in neat ethanol [19]. The aggregates formed in our case show θ values that lie somewhere between 0° and 180°, thus perfect H- or J-aggregates are not formed. This deviation from perfect stacking in card-pack manner or head-to-tail arrangement may be a result of the structure of FL dye itself. As seen from Scheme 1, the benzoic acid part will remain out of the plane of the anthracene moiety and will thus prevent perfect stacking, i.e., H-aggregation. That perfect J-aggregates (with $\theta = 180°$) are not formed can be seen

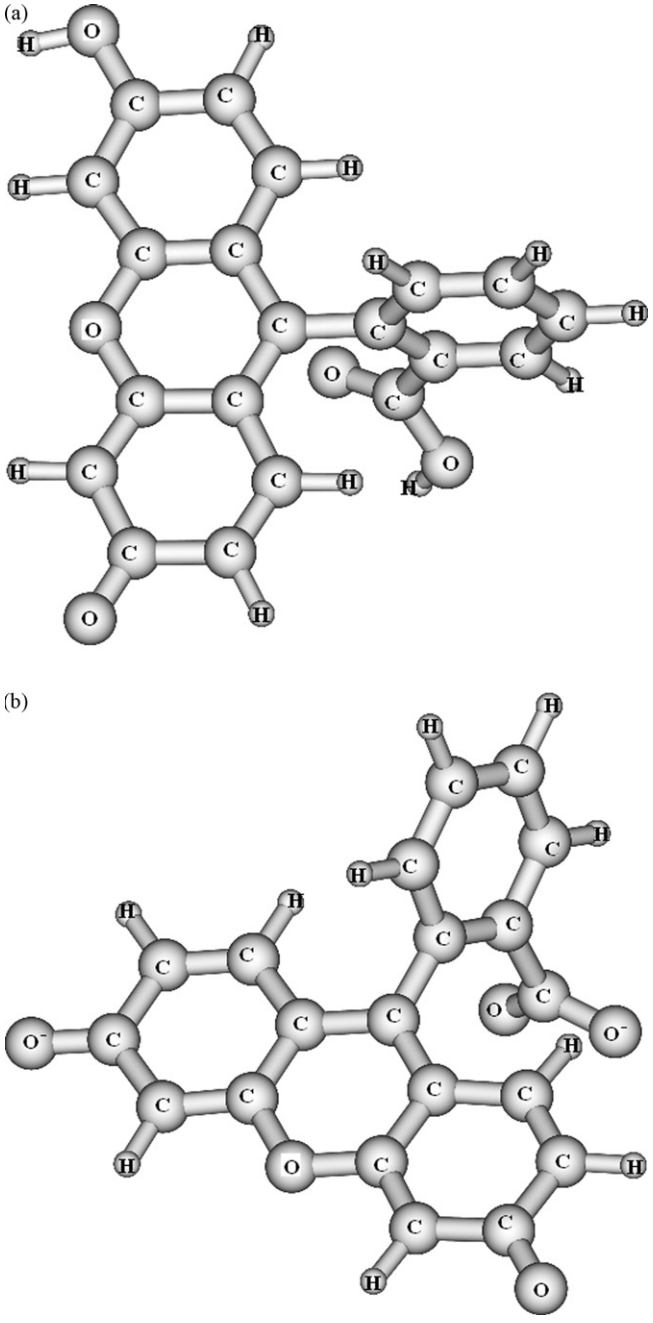

Scheme 1. Geometry optimized structure of (a) neutral FL molecule and (b) FL dianion.

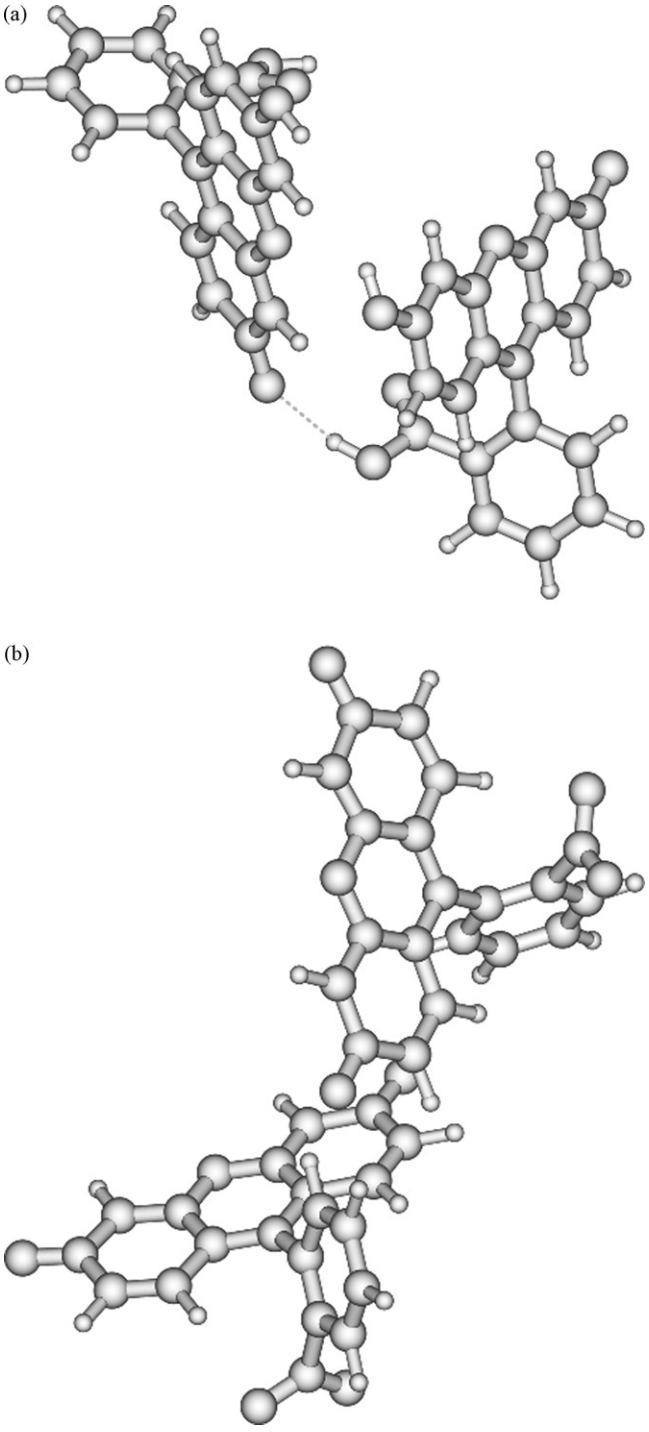

Scheme 2. Geometry optimized structure of (a) J-aggregates of neutral FL and (b) FL dianion.

from Scheme 2, which gives geometry-optimized structures of possible J-aggregates.

The results of the electronic structure calculations are shown in Table 2. The usual caveat regarding applicability of such calculations hold in the present case, i.e., (i) the calculations were all carried out in the gas phase, (ii) geometry optimization was at AM1 level, while DFT (and TDDFT) calculations were essentially single point, (iii) geometries of dimers were obtained as samples of more hybrid calculations (MD and AM1). Given such constraints, let us apply the data from Table 2 in our analysis of the spectra. The theoretical calculation on the dianion predicts peaks at 490, 432 and 417 nm. These correspond approximately to the peaks obtained in the experimental absorption spectrum of the dianion (except for the 432 nm peak which appears red-shifted in the experimental spectrum). The theoretical spectrum consists of π–π^* transitions of the anthracene moiety of the fluorophore. Twenty-eight nanometer red shift of the λ from the theory to the experimental case for the 432-nm peak may be due to solvent effects.

Table 2
Results of theoretical calculations on fluorescein dianion

Dye species	Transition energy (eV)	Corresponding λ (nm)	Observed λ_{max} (nm)
Monomer	2.529	490.2	490
	2.870	432.0	460
	2.969	417.6	420
Dimer			
J-type	2.309	537	505–540
H-type	2.932	422.8	460–400

For the dimers, it was difficult to calculate transition energies by TDDFT with the available computational facility. However we could arrive at possible structures for the dimers based on AM1 calculations. One of the many possible stable structures for the J-type dimers formed by neutral FL and FL dianion are shown in Scheme 2. Table 2 shows the results of TDDFT calculations on some dimers formed by FL dianion. For the J-type dimer, theory predicts λ_{max}^{abs} to be ~537 nm. Experimentally, we have obtained the J-type aggregate spectrum within the range 505–540 nm (in the experimental case, it is difficult to specify the actual λ_{max}^{abs} for the dimer). However, we note that on a broader level, there is a good correspondence between the theoretically predicted value of λ_{max}^{abs} and the experimentally obtained value for the J-type dimer. For the H-type dimer, Table 2 predicts λ_{max}^{abs} to be ~423 nm while our experiments indicate the H-type aggregate λ_{max}^{abs} range to be 460–400 nm. Thus we find that there is reasonable correspondence between the theoretically calculated values of the transition energies and the experimentally obtained values (from absorption spectra) for the species under study, i.e., the monomer dianion.

For fluorescence studies, the samples were excited at the main absorption peak of fluorescein, i.e., 490 nm corresponding to the dianion absorption. In a set corresponding to a fixed dye concentration, the emission spectra were studied in the presence of increasing NaDC concentrations. λ_{em} of FL in buffer at pH 6 is at 511 nm. For low-dye concentrations, i.e., 1×10^{-6} to 7×10^{-6} M FL, addition of increasing amounts of NaDC leads to slight increase in fluorescence intensity by about 10% at 40 mM NaDC, along with a red shift of about 2–5 nm in λ_{em}. Fluorescence excitation spectra resemble the ground state absorption spectra with the 460 nm shoulder disappearing with increasing NaDC concentrations. It is worth mentioning here, that on exciting the dye/gel at 450 and 505 nm, i.e., wavelengths corresponding to where the dye aggregates absorb (as discussed earlier) fluorescence intensity was lower than that for 490 nm excitation indicating that at these dye concentrations the

Table 3a
Lifetime studies of FL with varying NaDC at pH 6

System	a_1	τ_1 (ns)	a_2	τ_2 (ns)	χ^2
1×10^{-6} M FL					
FL	1	3.79			1.16
FL + 10 mM NaDC	0.13	4.08	0.87	0.12	1.27
3×10^{-5} M FL					
FL	1	3.68			1.2
FL + 10 mM NaDC	0.56	4.08	0.44	0.23	1.1
1×10^{-4} M FL					
FL	0.9	4.69	0.1	0.91	1.16
FL + 10 mM NaDC	0.55	4.86	0.45	0.30	1.2
FL + 40 mM NaDC	0.61	5.29	0.39	0.27	1.18
1×10^{-3} M FL					
FL	0.62	5.92	0.38	0.42	1.09
FL + 10 mM NaDC	0.57	6.3	0.43	0.31	1.02
FL + 40 mM NaDC	0.56	6.89	0.44	0.22	1.19

predominant species is the monomer dianion. The lifetime values of FL at various NaDC gel concentrations are given in Table 3a. At low-dye concentrations, i.e., 1×10^{-6} M, the fluorescence decay of FL in neat buffer is single exponential with a decay constant of 3.8 ns, consistent with the reported values [27]. At this dye concentration, in the gel, fluorescence decay is biexponential with major contribution from a fast component, i.e., 120 ps and a minor component of 4 ns. The latter value is the time constant for decay of dye monomer fluorescence. The origin of the fast component will be discussed later.

At moderately high-dye concentrations (1×10^{-5} to 1×10^{-4} M), there is larger fluorescence enhancement in the gel, i.e., 30% at 40 mM NaDC. The red shift in λ_{em} is also much more. What is remarkable is the distinct splitting of the fluorescence excitation spectra ($\lambda_{em} = 555$ nm) of the neat dye solution into two bands—one sharp red-shifted band with a peak at ∼510 nm and one broad blue-shifted band of lower intensity centered at ∼430 nm. As discussed in the earlier section, the splitting of the excitation spectra implies the existence of two types of aggregates having geometry intermediate between perfect J and perfect H-aggregates [18a,21]. We had earlier named them as Type A (stacked aggregates) and Type B (head-to-tail aggregates). The PCA analysis of the absorption spectra discussed earlier yields components that tally with the split bands observed in the fluorescence excitation spectra. In the gel medium, fluorescence intensity at both these bands increases as was seen from the excitation spectra (not shown). Also the longer wavelength band gets red shifted in presence of NaDC gel. At these dye concentrations, the decay of dye in neat buffer is also single exponential like for low-dye concentrations (Table 3a). However, in presence of the gel, a shorter component of ∼230 ps (τ_2) contributes equally.

At very high-dye concentrations, i.e., 1×10^{-3} M (Fig. 2a), overall fluorescence intensity is low for the neat dye. However, in presence of the gel, there is a dramatic fourfold enhancement in I_{em} at 40 mM NaDC. The λ_{em} is slightly red shifted to ∼550 nm. The fluorescence excitation spectra show greater splitting ($\Delta\lambda$), i.e., of ∼130 nm—split peaks lying at 530 and 400 nm (Fig. 2b). These are assigned to higher Type B aggregates and Type A aggregates respectively. In the gel, emission intensity at both the peaks increases. At these dye concentrations, the fluorescence decay in neat buffer is bi-exponential with a component of 4–6 ns and a fast component of several hundred picoseconds (Table 3a). With increasing gel concentration, the picosecond component becomes shorter and its contribution increases.

We have also carried out fluorescence anisotropy studies on the NaDC gels. Steady state fluorescence anisotropy (r) was calculated in the usual way from the fluorescence intensity at parallel (I_{II}) and perpendicular (I_L) polarization. Table 4 shows the anisotropy values for different fluorescein concentrations at different concentrations of gel. Fluorescence anisotropy from a fluorophore in a rigid environment reveals information about its local environment. It is seen that r-values are very low (0.01–0.04) for the neat dye solutions at pH 6 and increase in the gel, indicating increased rigidity in the gel.

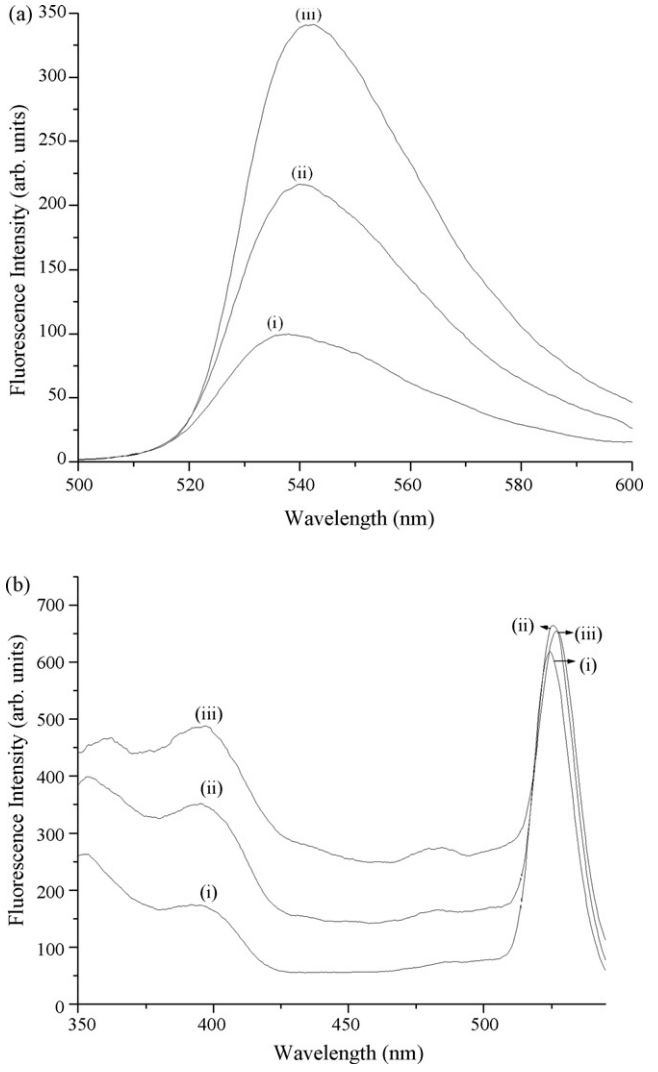

Fig. 2. (a) Fluorescence emission spectra of 1×10^{-3} M FL with varying NaDC at pH 6: (i) 0 mM, (ii) 10 mM, and (iii) 40 mM. (b) Fluorescence excitation spectra of 1×10^{-3} M FL with varying NaDC at pH 6: (i) 0 mM, (ii) 10 mM, and (iii) 40 mM.

As dynamic light scattering studies (DLS) have often served as an important tool to study and characterize gels as well as reverse micellar systems [29,30], DLS studies were undertaken to ascertain the hydrodynamic radii (R_h)/sizes of the particles formed by NaDC at pH 6 (Table 5). Interesting trends are observed in the DLS results. As NaDC concentration in the gel increases, the polydispersity index (PI) increases. In the gel, three types of scatterers are observed in DLS-i) one major population with $R_h \sim 70$–120 nm and two other types with $R_h \sim 5$–20 nm and $R_h \sim 5300$ nm. The particles with radii 5–20 nm may correspond to primary aggregates of NaDC while the bulk population of radius 110–120 nm corresponds, in all probability to secondary bile salt aggregates. That bile salts form primary and secondary aggregates in aqueous solution, is a well-established fact [5,6]. The largest aggregate with $R_h \sim 5300$ nm may correspond to the gel fibers, which are elongated in cross-section as reported in literature [9]. As NaDC concentration in the gel increases, this population of scatterers becomes dominant as can be seen from the amplitude of the peak at 40 mM NaDC (Table 5). The primary aggregates (5–20 nm in diameter) are almost non-existent in the gel while a substantial population of larger aggregates ($R_h \sim 67$ nm) is also present.

The Z-average diameter is the mean diameter based on the intensity of scattered light and is sensitive to the presence of aggregates/large particles. Since we observe a gradual increase in Z-average diameter from 512 to 1898 nm as NaDC concentration in the gel increases, we ascribe this to the formation of larger aggregates, i.e., gel fibers. Regarding the polydispersity of the sample, we find an increase of the PI with increasing NaDC concentration in the gel. The PI even at 10 mM NaDC is relatively high, i.e., 0.56 and it increases to 1 at 40 mM NaDC. Thus, the NaDC gel medium is quite polydisperse. The polydispersity is related to the heterogeneity in aggregate structure in terms of the aggregation number. For such a polydisperse sample (PI > 0.5), it is wiser to make comparative analysis based on the actual distribution rather than rely totally on the Z-average size. In our case, however, both the intensity distribution and the Z-average size indicate the same trend, i.e., increase in particle size with increasing gel concentration.

To further substantiate the findings from DLS studies, we carried out the studies of NaDC aggregates at pH 6 with an optical microscope. The resolution of the microscope is 0.5 μm, thus all structures present that have diameter ≥500 nm can be observed with fairly good precision. Indeed, we find that in the gel, long fibrous structures as reported in literature are seen (Fig. 3). The fibers become thicker and longer with increasing gel concentration.

3.2. Studies in NaDC micelles

In the neat aqueous buffer at pH 8.3, the absorption spectrum of FL indicates the presence of the FL dianion with a peak at 490 nm and a slight shoulder at 475 nm. At all dye concentrations, there is not much change in the short wavelength shoulder in the absorption spectrum of the dye, in presence of NaDC. This is in contrast to the interesting changes brought about in the absorption spectrum of FL by NaDC gel, as discussed earlier.

Fig. 3. Microscopic image of NaDC gel (40 mM), pH 6.

Like in absorption, NaDC at pH 8.3 has very little effect on the fluorescence emission and excitation spectra of FL. Increasing NaDC concentration gradually up to 40 mM leads to slight decrease in I_{em} with a small red shift in λ_{em}. Even when the fluorescence excitation spectra show distinct splitting (at [FL] $\geq 3 \times 10^{-5}$ M) indicating the presence of Type A and Type B aggregates, there is practically no change in emission intensity. Thus, NaDC at pH 8.3 has not as marked an effect on the spectral properties of FL as NaDC gel at pH 6 does.

The fluorescence decay of FL at low and moderately low-dye concentrations is exponential in neat buffer at pH 8.3, $\tau = 4$ ns (Table 3b). At higher dye concentrations, i.e., [FL] $\geq 1 \times 10^{-4}$ M, the decay of neat dye is biexponential with a major component of ~5 ns and a minor component that is fast, i.e., 540 ps (Table 3b). In presence of NaDC micellar aggregates, the traces are again biexponential with decay time of 4–5 ns along with a growth component of 150–200 ps. The growth component is indicated by negative amplitude. Such similar growth in fluorescence decay was also observed earlier for FL in NaDC and NaC micelles [18b].

Table 3b
Lifetime studies of FL with varying NaDC at pH 8.3

System	a_1	τ_1 (ns)	a_2	τ_2 (ns)	χ^2
1×10^{-6} M FL					
FL	1	3.99			1.35
FL + 10 mM NaDC	−0.07	0.19	1.07	4.13	1.12
FL + 40 mM NaDC	−0.08	0.12	1.08	4.22	1.10
3×10^{-5} M FL					
FL	1	4.17			
FL + 10 mM NaDC	−0.58	0.16	1.58	4.40	1.20
FL + 40 mM NaDC	−0.57	0.18	1.57	4.40	1.29
1×10^{-4} M FL					
FL	0.3	0.54	0.70	5.64	1.16
FL + 10 mM NaDC	−0.53	0.23	1.53	5.69	1.30
FL + 40 mM NaDC	−0.52	0.24	1.52	5.84	1.18

Table 4
Steady-state anisotropy studies of FL with varying NaDC

pH	[FL] (M)	[NaDC] (mM)	Anisotropy
6	1×10^{-6}	0	0.04
		10	0.07
		20	0.06
		40	0.08
	1×10^{-4}	0	0.02
		10	0.06
		20	0.11
		40	0.11
	1×10^{-3}	0	0.01
		10	0.10
		20	0.14
		40	0.12
8.3	1×10^{-6}	0	0.02
		10	0.03
		20	0.04
		40	0.05
	1×10^{-4}	0	0.01
		10	0.02
		20	0.03
		40	0.01
	1×10^{-3}	0	0.01
		10	0.01
		20	0.04
		40	0.02

Also, the increase in anisotropy (r-value) with NaDC concentration is greater in the gel than at pH 8.3 as seen from Table 4. This is expected as NaDC forms normal micelles at pH 8.3 and these micelles are less rigid than the gel (as indicated by the very low r values).

DLS studies were performed with the NaDC micelles. Table 5 shows that at pH 8.3, particle diameters are in the range 140–270 nm. Some smaller structures of ~1–2 nm diameter are also seen. The structures with R_h 1–2 nm seen in DLS are probably NaDC micelles formed at this pH, (with 0.6 nm instrumental resolution 1–2 nm structures may be detected quite accurately). Generally micelles formed from conventional surfactants have diameters ranging between ~30 and 50 Å, i.e., 3–5 nm [30b]. Also DLS experiments performed by Mukhopadhyay et al. reveals that the mean hydrodynamic radius of sodium cholate micelles is 1.2 nm [15b]. However, we see from Table 1 that these structures give a minor contribution to scattering. The major contribution comes from the structure having $R_h \sim 140$–270 nm. These are the secondary aggregates formed from the primary bile salt micelles.

4. Discussions

4.1. NaDC gel

At pH 6 in NaDC gel, we have observed a shoulder at 460 nm and the main peak at 487 nm in the absorption spectra of FL at micromolar concentrations. The 487 nm peak is well characterized for FL and arises due to monomer dianion absorption. The 460 nm shoulder needs to be assigned. Following a separate pH dependent study of the absorption spectra, we note that increasing the pH above 6 gradually leads to suppression of the 460 nm shoulder. Sjoback et al. [28b] has performed a detailed study of the protolytic equilibria of FL. They have shown that at pH ~ 6.14, both the anion and dianion are present. They have mentioned that the dianion has its main absorption peak at 490 nm with a shoulder around 475 nm while the anion has somewhat weaker absorption in the visible region with peaks at 472 nm and 453 nm of roughly the same molar absorptivity. We have calculated the pH-dependent difference absorption spectra (DAS) [19] of FL by subtracting the spectra of FL at pH 8.3 from the spectra at pH 6 (Fig. 4). This is expected to show the existence of any additional species that maybe present at pH 6 but absent at pH 8.3. Such a difference absorption spectrum resembles the absorption spectrum of FL anion (Fig. 4) as reported by Sjoback et al. [28b] with peaks of similar optical density at 470 and 450 nm. Thus, we assign the 460 nm shoulder, observed in the absorption spectrum of 1×10^{-6} M FL at pH 6, to the monomer anion absorption. In the NaDC gel, the 460 nm shoulder at pH 6 decreases with a concomitant rise in absorbance at 490 nm and a narrowing of the absorption spectrum (Fig. 1b). Now, it is known that the gelation process uptakes H^+ from the surrounding medium [7b]. It has been reported that during gelation, the gel fibers uptake H^+ and replace Na^+ ions in the network by these H^+ ions. As a result the local pH in the surrounding medium may increase. This will shift the FL anion $\rightleftharpoons$ dianion equilibrium to the RHS. In our case, thus the anion absorption around 450–470 nm decreases with a concomitant increase in dianion absorbance at 490 nm. Other workers too, have reported that the micellization of bile salts induces H_3O^+ binding [31a]. Sugihara et al. have also reported that an uptake of H^+ has been observed to occur during gel formation [31b]. However there is one important point that should not be overlooked. We can exclude the contribution of FL aggregates to the shoulder at 460 nm from the simple reasoning given as follows. At very low-FL concentrations, i.e., 1×10^{-7} M, chances of aggregate formation are nil. We have observed that the absorption spectra of 1×10^{-7} and 1×10^{-6} M FL at pH 6 are overlapping. Thus, in all prob-

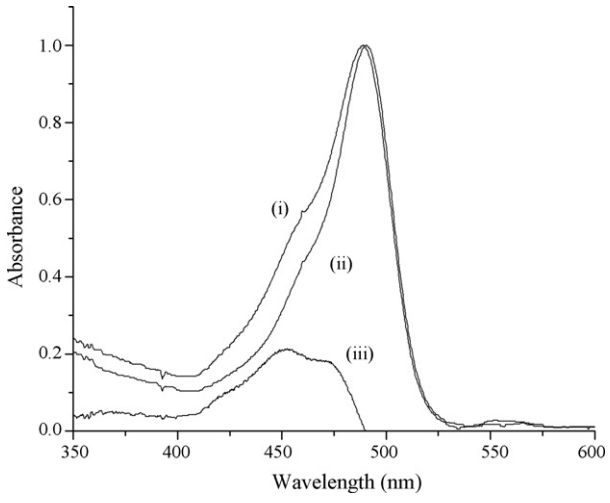

Fig. 4. Normalized absorption spectra of 1×10^{-6} M FL at two different pHs: (i) pH 6, (ii) pH 8.3, and (iii) the difference (i)–(ii) absorption spectra showing spectra of FL anion.

Table 5
Results of dynamic light scattering for NaDC gel and NaDC micelles

Sample	Temperature, T (°C)	Z-average (nm)	PI	Peak 1 (nm)	Peak 2 (nm)	Peak 3 (nm)	Contribution of peak 1	Contribution of peak 2	Contribution of peak 3
pH 8.3									
10 mM NaDC	25	296.1	0.33	1.18	16.82	147.6	0.03	0.18	0.79
40 mM NaDC	25	613.6	0.53	1.21	0	277.5	0.22	0	0.78
pH 6									
10 mM NaDC	25	512.5	0.56	13.6	112.2	5390	0.12	0.73	0.15
20 mM NaDC	25	611.2	0.65	21.8	119.2	5493	0.20	0.68	0.12
40 mM NaDC	25	1898	1.00	5.2	67.14	5249	0.06	0.39	0.55

ability, the shoulder at 460 nm does not derive any contribution from FL aggregates for low-dye concentrations. Summarizing, at low-dye concentrations, the gel medium promotes the conversion of existing dye monomer anions to monomer dianions due to H^+ uptake.

The steady-state fluorescence results also lend support to our existing idea that at pH 6, the neat dye solution consists of both anions and dianions. In presence of the gel, anions get converted to the dianions. Also, there are no H-type aggregates at these low-dye concentrations. The fluorescence excitation spectra resemble the absorption spectra. However, the time-resolved fluorescence studies indicate the emergence of a major component of ~120 ps in the fluorescence lifetime of FL in the gel environment (Table 3a). This indicates the existence of J-type aggregates in the gel environment. Type B or aggregates with J-type geometry are generally fluorescent and have very short decay times [28a]. Thus, in addition to the effect of conversion of monomer anions to monomer dianions within the restricted gel environment, we must also include the possibility of gel-induced J-type aggregation in the FL monomers at these low-dye concentrations. These J-type aggregates are fluorescent, thus accounting for the 10% increase in emission intensity. The increase in the angle θ in the gel from 72° to 85° also hints at gel induced J-type aggregation in FL. The red shift in the emission spectra along with the narrowing of the absorption spectra lends support to this idea [28a]. The fluorescence anisotropy of FL increases from 0.04 to 0.08 in the gel indicating an increase in rigidity of the environment surrounding the dye.

At moderately high-dye concentrations, i.e., in the range 1×10^{-5} to 1×10^{-4} M, we have observed similar gel-induced decrease in the 460 nm shoulder accompanied by rise of absorbance at 490 nm and a distinct narrowing of the absorption spectrum. From earlier work on FL, it is known that FL forms aggregates (mainly dimers) in this concentration regime. The PCA analysis of the absorption spectra at these dye concentrations indicates two components at 455 and 500 nm. With increasing gel concentrations, the amplitude of the 500 nm component increases. Here too, we have calculated the difference absorption spectrum by subtracting the spectrum of the neat dye solution in buffer from the spectra in gel [25]. The difference absorption spectra Fig. 5 shows both positive and negative absorption bands identifying only such dye species, which are either formed or decomposed within the gel medium. We find that there are two bands in the DAS, one in the negative absorbance region with peak at 450 nm and one positive band with peak at 500 nm. The blue-shifted band at 450 nm is assigned to H-type or Type A aggregates while the red-shifted band at 500 nm is assigned to J-type or Type B aggregates. We see from Fig. 5, that with increasing gel concentration, there is depletion in the population of Type A aggregates accompanied by a subsequent enrichment in population of Type B aggregates as indicated by the difference absorption spectra. The θ value in this concentration range increases from ~70° to 80° as gel concentration increases indicating a transition from stacked geometry to head-to-tail geometry of the dye aggregates in presence of the gel. Thus, at moderately high-dye concentrations, NaDC gel promotes the formation of J-type or Type B aggregates and also causes conversion of the existing H-type aggregates to J-type aggregates. Berlepsch et al. [20] have also noted significant reduction of the blue-shifted band for the cyanine dye C_8O_3 in presence of PVA. These dyes are also known to form aggregates in solution. They have assigned the isosbestic point arising in presence of PVA to two types of aggregates co-existing in presence of PVA. Very early studies on NaDC gels have reported that in gel fibers, bile salt molecules assumed an elongated helical configuration, 36 Å in diameter [7]. In our case from an approximate calculation, the cross section of the fibers seen in Fig. 3 has

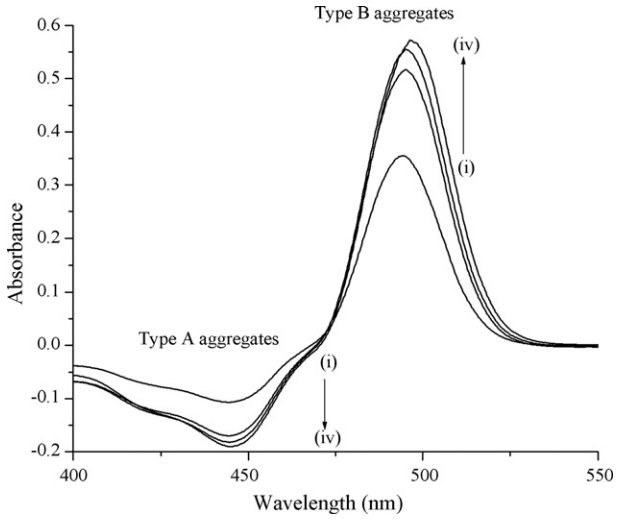

Fig. 5. Difference absorption spectra of 3×10^{-5} M FL with varying NaDC at pH 6: (i) 10 mM NaDC, (ii) 20 mM NaDC, (iii) 30 mM NaDC, and (iv) 40 mM NaDC.

Scheme 3. Proposed schematic for J-aggregation in NaDC gel.

a wide variation from the limited 0.6–11 μm. It must be noted that due to the limited resolution of our instrument, we will not be able to detect smaller structures. Our idea is that within such a confined space, stacking of dye monomers over one another will be prevented across the fiber cross-section, rather head-to-tail arrangement across the cross-section of the fibers will be preferred (Scheme 3). Even for the fiber with the smallest cross-section, i.e., 0.6 nm, the distance is much larger than the size of a FL monomer or dimer. Thus there is enough space for head-to-tail aggregation. Thus, at moderately high-dye concentrations Type B aggregates will be formed in preference to Type A aggregates. The fluorescence emission in these conditions arises due to fluorescent Type B aggregates. Increase in I_{em} in the gel occurs due to increase in percentage of fluorescent Type B aggregates in the gel, due to gel-induced conversion of existing Type A aggregates to Type B aggregates. The lifetime values (Table 3a) show the emergence of a picosecond component in the gel further hinting at gel induced J-aggregation.

For high-dye concentrations, i.e., 1×10^{-4} to 1×10^{-3} M, the absorption spectra are broad and PCA analysis yields two components at 450 and 505 nm. With increasing gel concentration, the amplitude of the 450 nm component decreases while that of the 505 nm component increases. The difference absorption spectra for 1×10^{-3} M FL (Fig. 6) however, indicate two well separated components at 420 and 520 nm. With increasing gel concentration, the 420 nm component gets depleted while the 520 nm component gets enriched. The much blue-shifted band at 420 nm indicates the formation of higher H-type aggregates. Similarly, the red-shifted sharp band at 520 nm indicates the formation of higher head-to-tail type aggregates. Table 1 indicates that the average angle at such high-dye concentrations in neat solution is generally low ∼55°. This is a general observation for the aggregation of most dyes, i.e., as dye concentration increases, stacking is preferred over head-to-tail arrangement [18a,19]. The obvious indication for the preferential stacking is a decrease in θ. Thus at very high-dye concentrations, Type A aggregates predominate in neat dye solution although Type B aggregates are also present. The contribution of the Type B aggregates increases with increasing NaDC concentration. At very high-dye concentrations, i.e., 1×10^{-3} M (Fig. 2a), overall fluorescence intensity is low for the neat dye due to the dominant population being non-fluorescent Type A aggregates. However, in the gel, fluorescence increases. For these high-FL concentrations, fluorescence decay of FL in neat buffer itself is not single exponential but bi-exponential with components of ∼5 ns and 200–400 ps. These components can arise due to the fluorescence decay of higher dye aggregates formed at these dye concentrations.

The low r values at pH 6, indicate a significant depolarization of the excited FL dipoles in solution. Such low r values maybe caused by rotational diffusion of the fluorophore and resonance energy transfer (RET) among the FL molecules. FL is highly susceptible to energy transfer due to the small Stokes' shift between its absorption and emission maxima. Probably this is also the reason why r-values decrease as FL concentration increases (Table 4). In presence of the gel at pH 6, r values for FL increase substantially. This increase in r may arise due to prevention of rotational diffusion of the fluorophore in the rigid gel medium. We also note that the gel-induced increase in r is higher for higher dye concentrations. This could be because at high-FL concentrations, the predominant species are higher H and J-aggregates with well-separated absorption and emission maxima. Thus due to reduced overlap, RET is prevented leading to a higher r value. Thus anisotropy studies too, lend support to the idea of enhanced aggregation in gel.

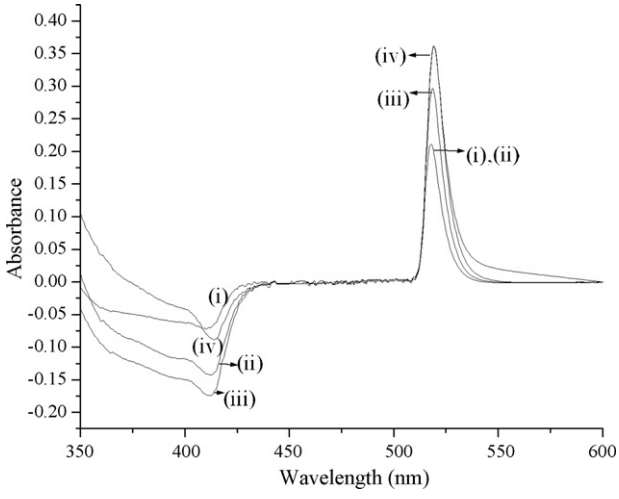

Fig. 6. Difference absorption spectra of 1×10^{-3} M FL with varying NaDC at pH 6: (i) 10 mM NaDC, (ii) 20 mM NaDC, (iii) 30 mM NaDC, and (iv) 40 mM NaDC.

The effect of NaDC gel on the dye aggregates could be explained by alteration of H-bonding within the aggregates, by the gel network. For aggregation of fluorescein monomers, H-bonding of dye molecules to the solvent is found to play an important role [18a,27]. Now, it is known that during gel formation by bile salts, there is a rearrangement of H-bonds within the gel network [7]. Blow and Rich have shown that there is an uptake of H^+ during the gel formation by NaDC, by using an automatic titrator. They believe that at low pH, a specific system of hydrogen bonding becomes possible within the micelle, leading to formation of a network with a regular internal order. At the molecular level, it appears that on lowering pH some of the deoxycholate ions can add protons, which neutralize their charge but without being precipitated as the insoluble deoxycholic acid. Instead they are arranged into the helical structure. Probably such uncharged –COOH groups are located in the inner hydrophobic part of the structure. It is most likely that the extra proton is used to form an H bond thus allowing the particle to grow. Although gel formation is some kind of aggregation, it is different from micelle formation in the sense that there is a specific requirement for molecular structure. Presence of 3-α-OH group favors gel formation, as this position is favorable for H-bonding in steroids. X-ray studies show that gels have a definite internal structure unlike micelles. The common picture of the NaDC gel is a helical fiber in which van der Waals stacking of steroid molecules and the O-H···O H-bonds play an important part. The COO^- groups lie on the cylindrical surface of the gel fibers but some of these may uptake H^+ and form –COOH which can participate in H-bonding both with other NaDC molecules and with the dye, FL. Thus the NaDC gel-induced changes of the molecular packing within the dye aggregates, as reflected by spectral changes, could be due to a rearrangement of these H-bonds.

Thus summarizing, we can say that at low-dye concentrations, the neat dye solution has both monomers (dianion and anion). In presence of gel, the anions get converted into dianions due to uptake of H^+ by the gel. Some J-type aggregates are also formed from the monomers. Thus fluorescence intensity increases a little (10%) and a short component arises in the fluorescence decay. Also θ values increases from 73° to 80°. At high-dye concentrations, the effect of the gel environment is more pronounced. Here, the neat dye solution is dominated by higher Type A aggregates, also some higher Type B aggregates are present. Thus at very high-dye concentrations, overall fluorescence of the dye is lower than at the intermediate dye concentrations due to non-fluorescent higher Type A aggregates being present. Here, the gel fibers promote the deaggregation of higher Type A aggregates at the same time promoting the formation of more Type B aggregates. Thus, there is a pronounced increase in fluorescence due to some of the non-fluorescent Type A aggregates being converted to Type B aggregates. This indicates that the gel medium can induce J-type aggregation in FL. In the time-resolved fluorescence studies, the faster component is due to a new species being created in the gel, i.e., Type B aggregate. Earlier workers have also reported fast non-exponential decays for J-aggregates of THIA-carbocyanine dyes in polyelectrolytes [28a,32]. They have more specifically assigned the fast component to energy transfer to trap or defect sites in the J-aggregate.

In the DLS studies, the large particles ($d \sim 5000$ nm) seen only in the gel at pH 6, may correspond to fibrous aggregates existing in NaDC gel network. Also the polydispersity for the gel is very high, i.e., ∼1 at high-gel concentrations indicating a wide variety in the population of scatterers. Rich and Blow [7] and others [3] have indicated that in the gel, NaDC aggregates are represented by helices. The gel is characterized by a bimodal R_h distribution, corresponding to very small and very big aggregates. Our DLS studies have also indicated such a distribution of very big and very small aggregates. The Cryo-TEM images also show that the gel network is made up of thin, flat ribbons [9]. That they are truly flat ribbons can be inferred from the uniform contrast for each one of them [9b]. This fact strongly supports our idea that the flat gel fibers facilitate the formation of dye aggregates in the head-to-tail geometry in a ribbon-like manner rather than dye stacking across the fibers.

4.2. pH 8.3

In the NaDC micelles at pH 8.3, at high-dye concentrations both Type A and Type B aggregates exist but NaDC does not lead to deaggregation of Type A aggregates, thus maintaining status quo. Also at low-dye concentrations, there is no marked change in the absorption spectra or fluorescence spectra in NaDC micelles. The time-resolved fluorescence studies indicate a growth component of several hundred picoseconds in NaDC micelles. In an earlier work we had explained how the growth could be rationalized in terms of dynamic aggregation of bile salt micelles to form larger aggregates [18b]. FL fluorescence reports faithfully on this aggregation process. We may note here that no such growth is observed in case of NaDC gel. Comparison of the results for gel and micelles shows that in the latter, i.e., at pH 8.3, no fast ps decay component is observed as in gel. Since this fast decay is characteristic of Type B or J-type aggregates under these conditions, we conclude that NaDC micelles do not promote the growth of Type B aggregates to the same extent as the gel. So, whatever happened in NaDC gel was an effect of gel network only and not the effect of the bile salt.

Due to the non-fluorescent Type A aggregates predominating at pH 8.3, fluorescence does not increase with NaDC. The small fluorescence decrease is due to transfer of monomer to the micellar interior. In such a situation, with increasing dye concentration, H-type aggregates are the natural choice. These being non-fluorescent, NaDC at pH 8.3 does not cause much fluorescence enhancement. It is known that bile salts being amphiphilic molecules form micelles in aqueous solutions. The micellization behavior of bile salts is known to be more complex than that of common surfactants as bile salts exhibit stepwise aggregation [5,18b,31]. Small angle X-ray scattering (SAXS) and small angle neutron scattering (SANS) studies of NaDC secondary aggregates show the existence of elongated rods with a central hydrophilic core filled with water [33–35]. Thus structurally, micellar aggregates of NaDC are quite different from NaDC gel fibers. This could explain the difference in their behavior. FL-aggregates, both Type A and Type B can be well stabilized

within the central water-filled hydrophilic core of NaDC secondary aggregates. Thus there is no need for disruption of Type A aggregation in presence of NaDC micelles. We believe that FL binds to secondary sites in the bile salt aggregates, which resembles conventional guest-micelle binding [36].

Comparison of the DLS results at the two different pHs shows that at pH 8.3, particle diameters are in the range 140–800 nm whereas, at pH 6, particle diameters can also reach very high values, i.e., 5000 nm.

5. Conclusions

Due to the importance of NaDC hydrogels in biomedical applications, there have been quite a few studies on these hydrogels over the last few decades. We were interested to examine the effect of these hydrogels on the aggregation behavior of the well-known xanthene dye, FL. Our results lead us to conclude that aggregation of Fluorescein does indeed occur in the gel environment. However, our most important finding is that within the gel medium, J-type aggregation is promoted, often at the expense of H-type aggregation. At low-dye concentrations, monomers are converted to Type B or J-type aggregates. At high-dye concentrations, Type A (H-type) aggregates are converted to Type B (J-type) aggregates. We have demonstrated a method for the preferential formation of J-aggregates of the xanthene dye FL. This result could have very important applications as thus far, only cyanine dyes have shown a strong tendency to form J-aggregates. We have shown that other dyes can also preferentially form J-aggregates in suitable media. We have, for the first time shown that the J-aggregate/H-aggregate ratio in the FL system can be "controlled" by regulating the properties of the bulk medium.

Our results are also important from the viewpoint of the material itself, i.e., NaDC hydrogel. By showing that the transformation H-aggregate → J-aggregate is promoted in gel media, we have lent support to the existing idea of gel formation by self-assembled fibrillar network (SAFIN) formation. It can also be realized that the hydrogel formed by NaDC has a microstructure very different from normal NaDC micelles, in accord with existing ideas about these systems.

Acknowledgements

S. Das thanks the University of Kalyani for financial assistance in the form of a university research fellowship. S. De thanks CSIR, New Delhi for generous grant of the Scheme 01 (1819)/02/EMR-II. We are grateful to Prof. K. Bhattacharyya of IACS, Kolkata for letting us perform the time-resolved fluorescence experiments at the set-up under DST project no. IR/I-1-CF-01/02. We acknowledge Prof. A Dasgupta for letting us use the DLS facility at CU, Kolkata. University of Kalyani is acknowledged for providing the basic infrastructure for research.

References

[1] P.P. Nair, D. Kritchevsky (Eds.), Bile Acids: Chemistry, Physiology and Metabolism, vol. 1, Plenum Press, New York, 1971.
[2] P.P. Nair, D. Kritchevsky (Eds.), Bile Acids: Chemistry, Physiology and Metabolism, vol. 2, Plenum Press, New York, 1973.
[3] S. Mukhopadhyay, U. Maitra, Curr. Sci. 87 (2004) 1666–1683.
[4] P. Schurtonburger, B. Lindeman, Biochemistry 24 (1985) 7161–7165.
[5] C. Ju, C. Bohne, J. Phys. Chem. 100 (1996) 3847–3854.
[6] G. Li, L.B. Mc Gown, J. Phys. Chem. 98 (1994) 13711.
[7] (a) A. Rich, D.M. Blow, Nature 182 (1958) 423;
(b) D.M. Blow, A. Rich, J. Am. Chem. Soc. 82 (1960) 3566.
[8] P. Terech, R.G. Weiss (Eds.), Molecular Gels, Kluwer, The Netherlands, 2004.
[9] (a) U. Maitra, S. Mukhopadhyay, A. Sarkar, P. Rao, S.S. Indi, Angew. Chem. Int. Ed. Engl. 40 (2001) 2281;
(b) S. Mukhopadhyay, U. Maitra, G. Krishnamoorthy, J. Schmidt, Y. Talmon, J. Am. Chem. Soc. 126 (2004) 15905.
[10] J.M. Guenet, Thermoreversible Gelation of Polymers and Biopolymers, Academic Press, New York, 1992.
[11] (a) L.A. Estroff, A.D. Hamilton, Angew. Chem. Int. Ed. 39 (2000) 3447;
(b) M. Suzuki, M. Yumoto, M. Kimura, H. Shirai, K. Hanabusa, Chem. Commun. (2002) 884.
[12] J.D. Hartgerink, E. Benaish, S.I. Stupp, Proc. Natl. Acad. Sci. U.S.A. 99 (2002) 5133.
[13] S. Bhattacharya, S.N.G. Acharya, Chem. Mater. 11 (1994) 3504.
[14] (a) R. Oda, I. Huc, S.I. Candau, Angew. Chem. Int. Ed. 37 (1998) 2689;
(b) F.M. Menger, A. Peresypkin, J. Am. Chem. Soc. 125 (2003) 5340.
[15] (a) P. Babu, D. Chopra, T.N.G. Rao, U.M. Maitra, Org. Biomol. Chem. 3 (2005) 3695–3700;
(b) S. Mukhopadhyay, I.G. Krishnamoorthy, U. Maitra, J. Phys. Chem. 107B (2003) 2189–2192.
[16] (a) T. Miyata, J. Uragami, K. Nakamac, Ad. Drug Deliv. Rev. 54 (2002) 79;
(b) K.Y. Lee, D.J. Moeny, Chem. Rev. 101 (2001) 1869.
[17] J.C. Tiller, Angew. Chem., Int. Ed. 42 (2003) 3072.
[18] (a) S. De, S. Das, A. Girigoswami, Spectrochim. Acta A 61 (2005) 1821–1833;
(b) S. De, S. Das, A. Girigoswami, Colloids Surf. B: Biointerf. 54 (2007) 74–81.
[19] R. Chaudhuri, F. Lopez Arbeloa, I. Lopez Arbeloa, Langmuir 16 (2000) 1285.
[20] H.V. Berlepsch, S. Kirstein, R. Hania, C. Didraga, A. Pugzlys, C. Bottcher, J. Phys. Chem. 107B (2003) 14176–14184.
[21] M. Kasha, M.A. El-Bayoumi, J. Phys. Chem. 34 (1961) 2181.
[22] (a) D.A. Higgins, P.J. Reid, P.F. Barbara, J. Phys. Chem. 100 (1996) 1174–1180;
(b) I. Yamazaki, N. Tami, T. Yamazaki, A. Murukami, M. Mimuro, Y. Fujita, J. Phys. Chem. 92 (1988) 5035;
(c) K. Minoshima, M. Taiji, K. Misawa, T. Kobayashi, Chem. Phys. Lett. 218 (1994) 67.
[23] (a) F.C. Spano, S. Mukamel, J. Chem. Phys. 91 (1989) 683;
(b) E.J. Sanchez, L. Novotny, X.S. Xie, Phys. Rev. Lett. 82 (1999) 4014.
[24] (a) H. Fidder, J. Terpstra, D.A. Wiersma, J. Chem. Phys. 94 (1991) 6895;
(b) V. Sundstrom, T. Gillbro, R.A. Gadonas, A. Piskarkas, J. Chem. Phys. 89 (1988) 2754.
[25] (a) C. Valenta, E. Nowack, A. Bernkop-Schnürch, Int. J. Pharm. 185 (1999) 103–111;
(b) Y.P. Sun, D.F. Sears Jr., J. Saltiel, F.B. Mallory, C.W. Mallory, C.A. Buser, J. Am. Chem. Soc. 110 (1988) 6974.
[26] (a) M.S. Gorden, M.W. Schmidt, in: C.E. Dykstra, G. Frenking, K.S. Kim, G.E. Senseria (Eds.), Theory and Applications of Computational Chemistry: The First Forty Years, Elsevier, Amsterdam, 2005, pp. 1167–1189;
(b) W.J. Stevens, H. Basch, M.K. Krauss, J. Chem. Phys. 81 (1984) 6026;
M. Krauss, H. Basch, P.G. Jesiew, Can. J. Chem. 70 (1992) 612;
T.R. Cundari, W.J. Stevens, J. Chem. Phys. 98 (1993) 5555;
(c) R.H. Hertwig, W. Koch, Chem. Phys. Lett. 268 (1997) 345.
[27] J.E. Selwyn, J.I. Steinfield, J. Phys. Chem. 76 (1972) 762.
[28] (a) E. Rousseau, M.M. Koetse, M. Van der Auweraer, F.C. De Schryver, Photochem. Photobiol. Sci. 1 (2002) 395;
(b) R. Sjöback, J. Nygren, M. Kubista, Spectrochim. Acta A 51 (1995) L7–L21.

[29] (a) D.B. Sellen, J. Polym. Sci. Polym. Phys. Ed. 25 (1987) 699;
(b) P.M. Burne, D.B. Sellen, Laser light scattering study of biological gels, in: S.A. Akhmanov, M. Yu (Eds.), Laser Applications in Life Sciences, vol. 1403, Poroshina SPIE, 1990, pp. 288–299.
[30] (a) R.A. Day, B.H. Robinson, J.H.R. Clarke, J.V. Doherty, J. Chem. Soc., Faraday Trans. II 75 (1979) 132–139;
(b) V.K. Aswal, P.S. Goyal, Chem. Phys. Lett. 368 (2002) 59.
[31] (a) S.C. De Sanctis, A.A.D. Archivio, L. Galantini, E. Gavuzzo, E. Giglio, J. Chem. Soc. Perkin Trans. 2 (2000) 403–407;
(b) G. Sugihara, M. Tanaka, R. Matuura, Bull. Chem. Soc. Jpn. 50 (1977) 2542.
[32] M. Horng, E.L. Quitevis, J. Phys. Chem. 97 (1993) 12408.
[33] S. Sen, P. Dutta, S. Mukherjee, K. Bhattacharyya, J. Phys. Chem. 106B (2002) 7745.
[34] A.A. D' Archivio, L. Galantini, E. Giglio, A. Jover, Langmuir 14 (1998) 4776.
[35] (a) G. Esposito, E. Giglio, N.V. Pavel, A. Zanobi, J. Phys. Chem. 91 (1987) 356;
(b) F. Lopez, J. Samseth, K. Mortensen, E. Rosenqvist, J. Rouch, J. Phys. Chem. 104B (2000) 197.
[36] C. Yihwa, F.H. Quina, C. Bohne, Langmuir 20 (2004) 9983–9991.